

Phonon anomalies in pure and underdoped $R_{1-x}K_x\text{Fe}_2\text{As}_2$ ($R=\text{Ba}, \text{Sr}$) investigated by Raman light scattering

M. Rahlenbeck¹, G. L. Sun¹, D. L. Sun¹, C. T. Lin¹, B. Keimer¹, and C. Ulrich^{1,2,3}

¹Max-Planck-Institut für Festkörperforschung, Heisenbergstraße 1, D-70569 Stuttgart, Germany

²University of New South Wales, School of Physics, 2052 Sydney, New South Wales, Australia and

³The Bragg Institute, Australian Nuclear Science and Technology Organization, Lucas Heights, NSW 2234, Australia

(Dated: October 30, 2018)

We present a detailed temperature dependent Raman light scattering study of optical phonons in $\text{Ba}_{1-x}\text{K}_x\text{Fe}_2\text{As}_2$ ($x \sim 0.28$, superconducting $T_c \sim 29$ K), $\text{Sr}_{1-x}\text{K}_x\text{Fe}_2\text{As}_2$ ($x \sim 0.15$, $T_c \sim 29$ K) and non-superconducting BaFe_2As_2 single crystals. In all samples we observe a strong continuous narrowing of the Raman-active Fe and As vibrations upon cooling below the spin-density-wave transition T_s . We attribute this effect to the opening of the spin-density-wave gap. The electron-phonon linewidths inferred from these data greatly exceed the predictions of ab-initio density functional calculations without spin polarization, which may imply that local magnetic moments survive well above T_s . A first-order structural transition accompanying the spin-density-wave transition induces discontinuous jumps in the phonon frequencies. These anomalies are increasingly suppressed for higher potassium concentrations. We also observe subtle phonon anomalies at the superconducting transition temperature T_c , with a behavior qualitatively similar to that in the cuprate superconductors.

PACS numbers:

The recent discovery of superconductivity in iron arsenides has triggered a large-scale research effort to explore the physical properties of these materials. After first reports on $\text{LaFeAs}(\text{O}_{1-x}\text{F}_x)$ with critical temperatures of $T_c = 26$ K [1] and 43 K under pressure [2], even higher transition temperatures up to 56 K were discovered in related compounds [3, 4]. LaFeAsO crystallizes in the ZrCuSiAs -type crystal structure [5] consisting of alternating $(\text{LaO})^+$ and $(\text{FeAs})^-$ layers with one $(\text{FeAs})^-$ layer per formula unit. In LaFeAsO , superconductivity is usually induced by substitution of F^- for O^{2-} , introducing electrons into the $(\text{FeAs})^-$ layers. It was recently shown that hole doping by substitution of La^{3+} for Sr^{2+} can also induce superconductivity with $T_c = 25$ K [6].

More recently a second class of iron arsenide superconductors crystallizing in the ThCr_2Si_2 -type crystal structure with two $(\text{FeAs})^-$ layers per formula unit was discovered [7]. The ternary iron arsenide BaFe_2As_2 (BFA) becomes superconducting after substitution of K^+ for Ba^{2+} , with $T_c = 38$ K at optimal doping ($x \sim 0.4 - 0.5$) [7, 8]. This system is a hole-doped superconductor. Isostructural compounds with Ca ($T_c = 20$ K) [9], Eu ($T_c = 32$ K) [10], and Sr ($T_c \sim 38$ K) [11, 12] instead of Ba followed soon thereafter. A first example of electron doping in a ternary iron arsenide, induced by substitution of Co^{2+} for Fe^{2+} in BaFe_2As_2 with $T_c = 22$ K, was reported as well [13]. In contrast to the oxypnictides, large high-quality single crystals are available for this class of compounds.

Common features of the undoped iron arsenide parent compounds are a structural phase transition from a high temperature tetragonal to a low temperature orthorhombic or monoclinic phase, and an antiferromagnetic spin-density-wave (SDW) transition. While for the electron-doped compounds both phase transitions were found at slightly different temperatures [14, 15], they oc-

cur at a same temperature T_s for hole-doped BKFA [8]. Undoped BaFe_2As_2 and SrFe_2As_2 show combined transitions at $T_s \sim 140$ K [16] and $T_s \sim 203$ K [17], respectively. Doping with electrons or holes suppresses T_s and induces superconductivity at lower temperatures. In hole-doped $R\text{Fe}_2\text{As}_2$ ($R=\text{Ba}, \text{Sr}$) strong indications exist for a distinct doping range where the superconducting and SDW phases coexist [8, 18]. In the coexistence regime of underdoped $\text{Ba}_{1-x}\text{K}_x\text{Fe}_2\text{As}_2$ (BKFA), there is evidence for a weaker structural transition at T_s without macroscopic change of the crystal symmetry, but with an increase of microstrains, that was attributed to a magnetically induced lattice softening in combination with electronic phase separation [19].

Raman light scattering offers a powerful tool to detect subtle changes in the phonon spectrum at structural or electronic phase transitions. In this work we present a detailed temperature dependent Raman light scattering study of the optical phonons in superconducting BKFA and $\text{Sr}_{1-x}\text{K}_x\text{Fe}_2\text{As}_2$ (SKFA) single crystals. We observe pronounced narrowing in the phonon linewidths at the combined phase transition temperature T_s , as well as more subtle phonon anomalies at the superconducting phase transition temperature T_c .

The experiments were performed on thin platelets of BKFA and SKFA single crystals (thickness ~ 20 μm) with the crystallographic c -axis perpendicular to the surface. The samples were grown from tin flux, as described previously [20, 21, 22]. They were underdoped with $x \sim 0.28$ and $x \sim 0.15$ (determined by energy-dispersive x-ray analysis and inductively-coupled plasma spectroscopy), respectively. From measurements of the electrical resistivity in the FeAs planes (Fig. 1) and the magnetization (Fig. 2) on samples from the same batch as the ones used for the Raman measurements, we infer superconducting transition temperatures $T_c \sim 29$ K

in both cases. In particular, the diamagnetic signal of SKFA shown in Fig. 2 is characterized by an onset of 32 K, a midpoint of 29 K, and a 10% – 90% width of 4 K. Similar data were previously reported for BKFA crystals from the same batch as ours [22]. The combined structural-SDW transition temperature in SKFA was determined as $T_s \sim 178$ K by a decrease of the in-plane resistivity on SKFA samples from the same batch [21], while $T_s \sim 75$ K was determined by neutron scattering and muon spin rotation experiments on BKFA samples from the same batch [22]. Furthermore, we used a non-superconducting sample of BFA with thickness ~ 50 μm grown in self-flux [21, 23], and $T_s \sim 138$ K inferred from the in-plane resistivity (Fig. 1).

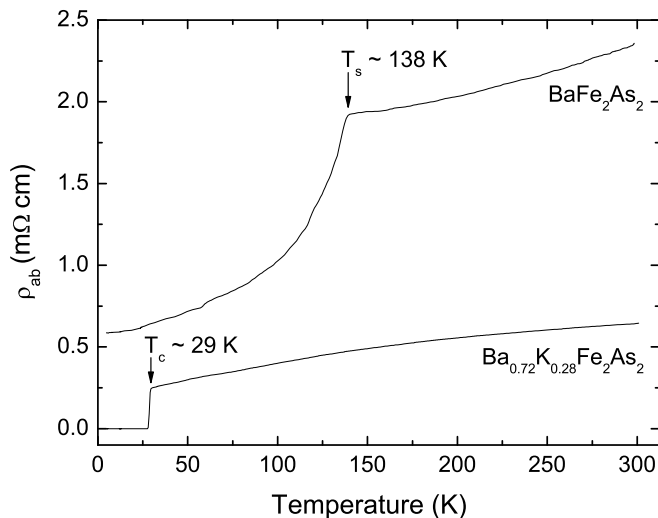


FIG. 1: In-plane resistivity of BFA and BKFA single crystals determined by a standard four-probe method.

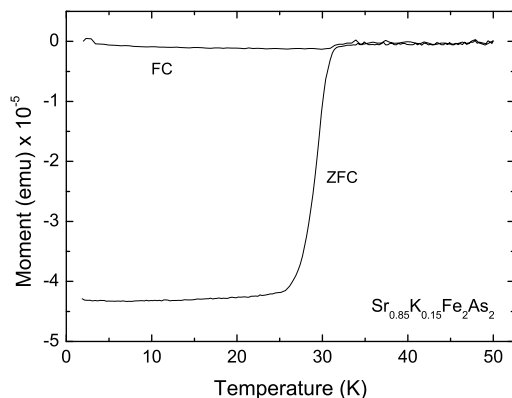


FIG. 2: Field-cooled (FC) and zero-field-cooled (ZFC) magnetization of a SKFA crystal in a magnetic field of 10 Oe applied along the crystallographic c -axis.

For the Raman measurements we used a micro-Raman

setup. The samples were mounted in a helium-flow cryostat, and the spectra were taken in backscattering geometry using the linearly polarized 632.817 nm line of a He^+/Ne^+ -mixed gas laser for excitation. The laser beam was focused through a $50\times$ microscope objective to a ~ 5 μm diameter spot on the sample surface. In order to avoid sample heating through the laser beam, we used an incident laser power of less than 1.5 mW. The scattered light was analyzed by a JobinYvon LabRam single-grating spectrometer equipped with a notch filter and a Peltier-cooled CCD camera. For each Raman spectrum an additional calibration spectrum of a nearby neon line was measured in order to determine the precise frequency and linewidth of the different phonons. For data analysis, all phonon peaks were fitted to Voigt profiles, which result from a convolution of the Lorentzian phonon line-shape with the instrumental resolution of ~ 2 cm^{-1} (full width at half maximum).

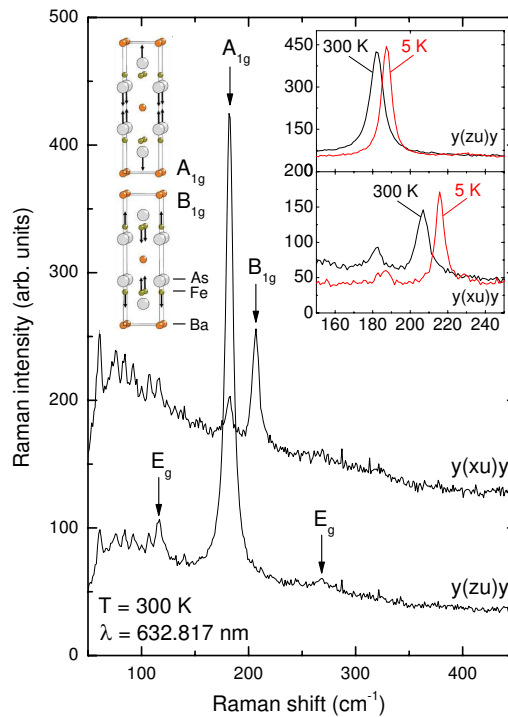


FIG. 3: Raman spectra of underdoped BKFA at 300 K in $y(xu)y$ and $y(zu)y$ polarization configurations. The additional peaks below ~ 150 cm^{-1} are artifacts of the optical setup. The insets show a comparison of the Raman spectra at 5 and 300 K. The displacement patterns show the Raman-active A_{1g} and B_{1g} modes as obtained from shell model calculations [24].

Figure 3 shows the Raman spectra of the underdoped BKFA single crystal at 300 K for the $y(xu)y$ and $y(zu)y$ polarization configurations. Here, we use the Porto notation $i(kl)j$, where i and j denote the direction of incident and scattered light and (kl) their polarization, respectively. In order to maximize the intensity, we did not use a polarization analyzer ($u = \text{unpolarized}$). From the tetragonal ThCr_2Si_2 -type crystal structure (space group

$I4/mmm$ (D_{4h}^{17}) one expects four Raman-active modes with symmetries $A_{1g} + B_{1g} + 2E_g$. According to the mode assignment of Litvinchuk *et al.* [24], the peaks at 182 cm^{-1} and 206 cm^{-1} can be identified with the A_{1g} and B_{1g} vibrations of the As- and Fe-atoms, respectively. The A_{1g} mode is strong for (zu) and weak for (xu) polarization, respectively. The B_{1g} mode cannot be observed for (zu) polarization in accordance with the Raman selection rules. The two E_g modes are weak and are observed at 117 cm^{-1} and 268 cm^{-1} in the y(zu)y polarization configuration. The insets show the corresponding Raman spectra at 5 and 300 K. All modes show a clear shift to lower energies upon heating from 5 to 300 K.

Figure 4 shows the frequency and full width at half maximum (FWHM) of the A_{1g} and B_{1g} modes of underdoped BKFA in the y(zu)y and y(xu)y polarization configurations as a function of temperature. The vertical lines correspond to the critical temperatures T_c and T_s for the superconducting and the combined structural-SDW transitions, respectively. Figure 5 shows corresponding data for underdoped SKFA ($x \sim 0.15$). Compared to BKFA ($x \sim 0.28$), the A_{1g} and B_{1g} modes are shifted to lower energies by $\sim 1 - 2 \text{ cm}^{-1}$ and $\sim 3 \text{ cm}^{-1}$, respectively, but the temperature evolution of the phonon parameters is closely similar in both samples.

The solid line through the B_{1g} data is the result of a fit to an expression based on phonon-phonon interactions, i.e. the anharmonic decay of phonons [25]. For simplicity we assumed a symmetric phonon decay according to:

$$\omega_{ph}(T) = -A \left(1 + \frac{2a}{\exp(\hbar\omega_0/2k_B T) - 1} \right) + \omega_0,$$

where A is a positive constant and a corrects for terms arising from non-symmetric phonon decay processes. While the frequency of the B_{1g} mode follows nearly perfectly the expression for anharmonic decay, significant deviations from this behavior are observed for the A_{1g} mode at both T_c and T_s . We first discuss the relatively subtle lineshape anomalies at T_c , and later turn to the stronger anomalies at T_s in the context of analogous measurements on non-superconducting BFA samples.

In contrast to the low-temperature saturation of the frequency of the B_{1g} modes, the A_{1g} modes of both BKFA and SKFA exhibit a distinct hardening by $\sim 0.3 \text{ cm}^{-1}$ upon cooling below T_c . Moreover, the linewidth of the A_{1g} mode in SKFA (Fig. 5) shows a kink in its temperature dependence at T_c , which can be described as a slight superconductivity-induced broadening superposed on a continuous decrease upon cooling below the spin-density-wave transition at T_s (to be discussed further below). While the latter trend is already nearly saturated at $T = T_c$ in SKFA, it is much more pronounced in BKFA, where T_s is considerably lower, and overshadows the superconductivity-induced linewidth anomaly (Fig. 4).

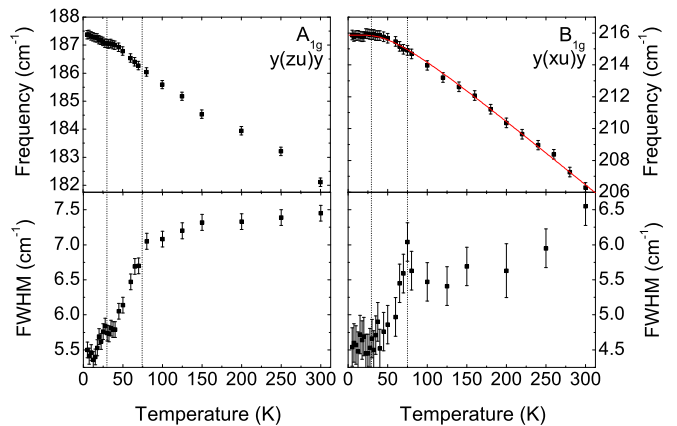


FIG. 4: Temperature dependence of the frequency and FWHM of the A_{1g} and B_{1g} modes in underdoped BKFA. The solid line is the result of a fit to the normal state data according to anharmonic phonon decay processes (see text for details). The dashed lines indicate the superconducting $T_c \sim 29 \text{ K}$ and the SDW transition temperature $T_s \sim 75 \text{ K}$ as obtained from Ref. 22.

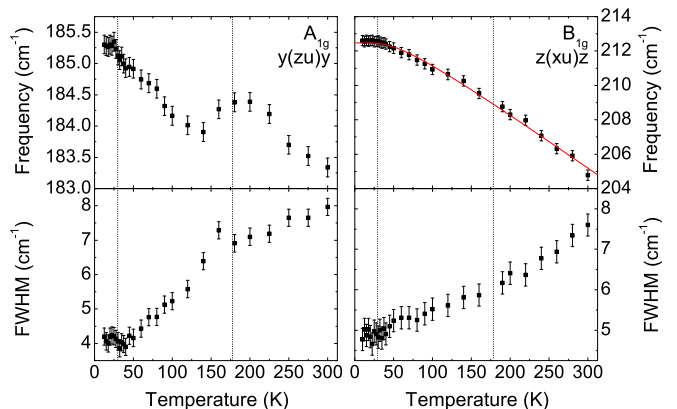


FIG. 5: Temperature dependence of the frequency and FWHM of the A_{1g} and B_{1g} modes in underdoped SKFA. The dashed lines indicate the superconducting $T_c \sim 29 \text{ K}$ and the SDW transition temperature $T_s \sim 178 \text{ K}$.

According to the standard description of superconductivity-induced self-energy anomalies of optical phonons [26, 27], the rearrangement of the electronic density of states below T_c is expected to induce hardening and broadening for phonons with energies above the pair-breaking energy 2Δ . Experimental observations on the cuprate high-temperature superconductors are largely consistent with this theory. Angle-resolved photoemission experiments on BKFA samples from the same batch as ours found two superconducting gap energies at $\Delta_1 \sim 9 \text{ meV}$ and $\Delta_2 \sim 4 \text{ meV}$ [28], yielding pair-breaking energies of $2\Delta_1 \sim 150 \text{ cm}^{-1}$ and $2\Delta_2 \sim 65 \text{ cm}^{-1}$. Assuming comparable gap values for the two BKFA and SKFA samples, both the A_{1g} and B_{1g} mode energies are well above the upper $2\Delta_1$ -gap. Our observations of a hardening and broadening in the

phonon frequency and linewidth at T_c are therefore in agreement with the theoretical expectations. The weakness of the observed self-energy renormalization indicates that the superconductivity-induced modification of the electronic density of states is small at the phonon energies monitored experimentally.

We now turn to the phonon anomalies at the combined structural-SDW transition temperature T_s . Beginning with the BKFA sample with the lowest T_s (Fig. 4), we note a pronounced singularity in the temperature dependence of the linewidths of both A_{1g} and B_{1g} modes at T_s , followed by a continuous narrowing upon cooling. This effect is further enhanced in the SKFA sample. The A_{1g} mode, in particular, narrows by $\sim 3 \text{ cm}^{-1}$ between T_s and the lowest temperature, and softens by $\sim 0.5 \text{ cm}^{-1}$ around T_s . For reference, we have carried out further experiments on pristine BFA, the results of which are shown in Fig. 6. Here the phonon anomalies at T_s are even stronger. The A_{1g} mode softens abruptly by $\sim 1 \text{ cm}^{-1}$ at T_s and narrows by more than $\sim 4 \text{ cm}^{-1}$ between T_s and the lowest temperature. The B_{1g} mode frequency also shows a small break in its temperature gradient at T_s , as well as a continuous narrowing by $\sim 2 \text{ cm}^{-1}$ between T_s and base temperature. Similar behavior was reported before for CaFe_2As_2 [29].

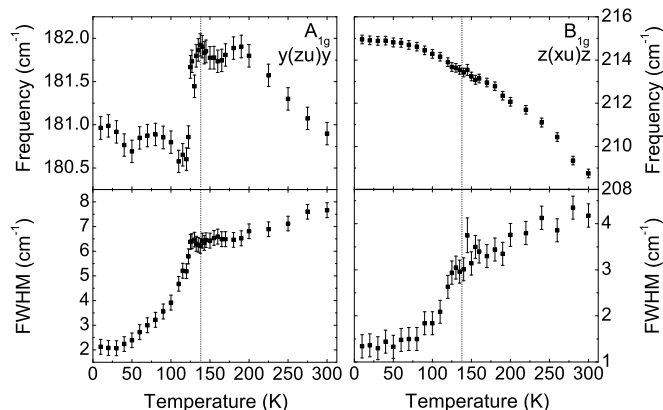


FIG. 6: Temperature dependence of the frequency and FWHM of the A_{1g} and B_{1g} modes in undoped BFA (grown in self-flux). The dashed lines indicate the structural-SDW transition temperature $T_s \sim 138 \text{ K}$ as obtained from Fig. 1.

In assessing the physical origin of the anomalies at T_s , we have to take into account the modification of the lattice structure and the opening of the SDW gap at this transition. As shown by several authors [30, 31, 32], the structural transition in the ternary iron arsenides tends to be of first order. The discontinuous jump in the frequency of the A_{1g} mode at T_s is consistent with this behavior and can be attributed to the contraction of the lattice at the structural transition [19]. The reduction of this discontinuity in the BKFA sample with the lowest T_s is in agreement with earlier experiments on BKFA samples from the same batch [19], where the structural phase transition was found to be macroscopically sup-

pressed. Note that recent Raman scattering measurements on electron-doped $\text{Ba}(\text{Fe}_{1-x}\text{Co}_x)_2\text{As}_2$ single crystals [33] revealed a splitting of the degenerate E_g in-plane modes at the tetragonal-to-orthorhombic transition.

On the other hand, the pronounced and continuous narrowing of both A_{1g} and B_{1g} modes below T_s cannot be understood as a consequence of the modification of the lattice structure and associated phonon-phonon interactions alone. It can, however, be understood if the difference between the linewidths above and below T_s is attributed to the electron-phonon interaction, which becomes inoperative at low temperatures due to the opening of the SDW gap [34]. This scenario is further supported by infrared experiments on EuFe_2As_2 single crystals [35], where the interaction of the Fe-As lattice vibration E_u with the electronic background was found to be reduced below the SDW transition. The continuous, second-order-like behavior of the linewidth can be reconciled with the abrupt jump in the phonon frequency either if separate first-order structural and second-order SDW transitions take place at slightly different temperatures that are not resolved in the experiment, or if the single, combined transition is weakly first-order so that the jump in linewidth is below the detection limit.

In any case, the strong reduction of the linewidths of both A_{1g} and B_{1g} modes below T_s points to a substantial influence of the electron-phonon interaction on the lattice dynamics in the iron arsenides. Ab-initio density functional calculations predict that the A_{1g} mode, which corresponds to a vibration of the arsenic ions along the c -axis, shows the strongest electron-phonon coupling [36, 37], in qualitative agreement with our observations. However, calculations without spin polarization fail to account quantitatively for the experimentally observed linewidths. The predicted [38] density of states at the Fermi level, $N(0) \sim 4.42/\text{eV}$, and total [36] electron-phonon coupling parameter (summed over the phonon branches and averaged on the Brillouin zone), $\lambda \sim 0.21$, yields a rough estimation for the FWHM [36, 39] of $\frac{1}{2}\pi N(0) \frac{\lambda}{15} \omega^2 \sim 0.4 \text{ cm}^{-1}$, about an order of magnitude smaller than observed for the A_{1g} mode above the SDW transition. This discrepancy is in line with earlier reports of differences between the calculated and observed phonon density of states around the A_{1g} mode energy [40, 41, 42, 43]. Since the ab-initio calculations also show that the electron-phonon coupling greatly increases in the SDW state [37, 44], this may be a manifestation of local Fe moments that survive well above the SDW transition.

In conclusion, we have shown that the electron-phonon coupling results in significant phonon anomalies at both the superconducting and spin-density-wave transitions of BKFA and SKFA. The anomalies at T_c are small, presumably because the phonon energies exceed the pair breaking energies, and consistent with the conventional theory of superconductivity-induced phonon self-energy modifications. The anomalies at T_s are much larger and qualitatively consistent with the opening of the spin-density-wave gap. A quantitative description of these

anomalies requires theoretical work beyond the density functional calculations thus far reported.

We would like to thank L. Boeri and M. Le Tacon for

fruitful discussions and A. Schulz for technical support during the Raman experiments.

-
- [1] Y. Kamihara, T. Watanabe, M. Hirano, and H. Hosono, *J. Am. Chem. Soc.* **130**, 3296 (2008).
- [2] H. Takahashi, K. Igawa, K. Arii, Y. Kamihara, M. Hirano, and H. Hosono, *Nature* **453**, 376 (2008).
- [3] C. Wang, L. Li, S. Chi, Z. Zhu, Z. Ren, Y. Li, Y. Wang, X. Lin, Y. Luo, S. Jiang, X. Xu, G. Cao, and Z. Xu, *Europhys. Lett.* **83**, 67006 (2008).
- [4] G. Wu, Y. L. Xie, H. Chen, M. Zhong, R. H. Liu, B. C. Shi, Q. J. Li, X. F. Wang, T. Wu, Y. J. Yan, J. J. Ying, and X.H. Chen, *J. Phys.: Condens. Matter* **21**, 142203 (2009).
- [5] V. Johnson and W. Jeitschko, *J. Solid State Chem.* **11**, 161 (1974).
- [6] H.-H. Wen, G. Mu, L. Fang, H. Yang, and X. Zhu, *Europhys. Lett.* **82**, 17009 (2008).
- [7] M. Rotter, M. Tegel, and D. Johrendt, *Phys. Rev. Lett.* **101**, 107006 (2008).
- [8] H. Chen, Y. Ren, Y. Qiu, W. Bao, R. H. Liu, G. Wu, T. Wu, Y. L. Xie, X. F. Wang, Q. Huang, and X. H. Chen, *Europhys. Lett.* **85**, 17006 (2009).
- [9] G. Wu, H. Chen, T. Wu, Y. L. Xie, Y. J. Yan, R. H. Liu, X. F. Wang, J. J. Ying, and X. H. Chen, *J. Phys.: Condens. Matter* **20**, 422201 (2008).
- [10] H. S. Jeevan, Z. Hossain, D. Kasinathan, H. Rosner, C. Geibel, and P. Gegenwart, *Phys. Rev. B* **78**, 092406 (2008).
- [11] G. F. Chen, Z. Li, G. Li, W.-Z. Hu, J. Dong, J. Zhou, X.-D. Zhang, P. Zheng, N.-L. Wang, and J.-L. Luo, *Chin. Phys. Lett.* **25**, 3403 (2008).
- [12] K. Sasmal, B. Lv, B. Lorenz, A. M. Guloy, F. Chen, Y.-Y. Xue, and C.-W. Chu, *Phys. Rev. Lett.* **101**, 107007 (2008).
- [13] A. S. Sefat, R. Jin, M. A. McGuire, B. C. Sales, D. J. Singh, and D. Mandrus, *Phys. Rev. Lett.* **101**, 117004 (2008).
- [14] H. Luetkens, H.-H. Klauss, M. Kraken, F. J. Litterst, T. Dellmann, R. Klingeler, C. Hess, R. Khasanov, A. Amato, C. Baines, M. Kosmala, O. J. Schumann, M. Braden, J. Hamann-Borrero, N. Leps, A. Kondrat, G. Behr, J. Werner, and B. Büchner, *Nature Materials* **8**, 305 (2009).
- [15] J.-H. Chu, J. G. Analytis, Ch. Kucharczyk, and I. R. Fisher, *Phys. Rev. B* **79**, 014506 (2009).
- [16] M. Rotter, M. Tegel, D. Johrendt, I. Schellenberg, W. Hermes, and R. Pöttgen, *Phys. Rev. B* **78**, 020503(R) (2008).
- [17] M. Tegel, M. Rotter, V. Weiß, F. M. Schappacher, R. Pöttgen, and D. Johrendt, *J. Phys.: Condens. Matter* **20**, 452201 (2008).
- [18] Y. Zhang, J. Wei, H. W. Ou, J. F. Zhao, B. Zhou, F. Chen, M. Xu, C. He, G. Wu, H. Chen, M. Arita, K. Shimada, H. Namatame, M. Taniguchi, X. H. Chen, and D. L. Feng, *Phys. Rev. Lett.* **102**, 127003 (2009).
- [19] D. S. Inosov, A. Leineweber, X. Yang, J. T. Park, N. B. Christensen, R. Dinnebier, G. L. Sun, Ch. Niedermayer, D. Haug, P. W. Stephens, J. Stahn, O. Khvostikova, C. T. Lin, O. K. Andersen, B. Keimer, and V. Hinkov, *Phys. Rev. B* **79**, 224503 (2009).
- [20] X.F. Wang, T. Wu, G. Wu, H. Chen, Y.L. Xie, J.J. Ying, Y.J. Yan, R.H. Liu, and X.H. Chen, *Phys. Rev. Lett.* **102**, 117005 (2009).
- [21] G. L. Sun, D. L. Sun, M. Konuma, P. Popovich, A. Boris, J. B. Peng, K.-Y. Choi, P. Lemmens, and C. T. Lin, arXiv: 0901.2728v2 (2009).
- [22] J. T. Park, D. S. Inosov, Ch. Niedermayer, G. L. Sun, D. Haug, N. B. Christensen, R. Dinnebier, A. V. Boris, A. J. Drew, L. Schulz, T. Shapoval, U. Wolff, V. Neu, X. Yang, C. T. Lin, B. Keimer, and V. Hinkov, *Phys. Rev. Lett.* **102**, 117006 (2009).
- [23] N. Ni, S.L. Bud'ko, A. Kreyssig, S. Nandi, G.E. Rustan, A.I. Goldman, S. Gupta, J.D. Corbett, A. Kracher and P.C. Canfield, *Phys. Rev. B* **78**, 014507 (2008).
- [24] A. P. Litvinchuk, V. G. Hadjiev, M. N. Iliev, B. Lv, A. M. Guloy, and C. W. Chu, *Phys. Rev. B* **78**, 060503(R) (2008).
- [25] J. Menéndez and M. Cardona, *Phys. Rev. B* **29**, 2051 (1984).
- [26] R. Zeyher and G. Zwirner, *Z. Phys. B - Condens. Matter* **78**, 175 (1990).
- [27] T. P. Devereaux, *Phys. Rev. B* **50**, 10287 (1994).
- [28] D. V. Evtushinsky, D. S. Inosov, V. B. Zabolotnyy, A. Koitzsch, M. Knupfer, B. Büchner, M. S. Viazovska, G. L. Sun, V. Hinkov, A. V. Boris, C. T. Lin, B. Keimer, A. Varykhalov, A. A. Kordyuk, and S. V. Borisenko, *Phys. Rev. B* **79**, 054517 (2009).
- [29] K.-Y. Choi, D. Wulferding, P. Lemmens, N. Ni, S. L. Budko, and P. C. Canfield, *Phys. Rev. B* **78**, 212503 (2008).
- [30] Q. Huang, Y. Qiu, W. Bao, M. A. Green, J. W. Lynn, Y. C. Gasparovic, T. Wu, G. Wu, and X. H. Chen, *Phys. Rev. Lett.* **101**, 257003 (2008).
- [31] N. Ni, S. Nandi, A. Kreyssig, A. I. Goldman, E. D. Mun, S. L. Budko, and P. C. Canfield, *Phys. Rev. B* **78**, 014523 (2008).
- [32] C. Krellner, N. Caroca-Canales, A. Jesche, H. Rosner, A. Ormeci, and C. Geibel, *Phys. Rev. B* **78**, 100504(R) (2008).
- [33] L. Chauvière, Y. Gallais, M. Cazayous, A. Sacuto, M. A. Méasson, D. Colson and A. Forget, arXiv: 0906.4569v1 (2009).
- [34] W. Z. Hu, J. Dong, G. Li, Z. Li, P. Zheng, G. F. Chen, J. L. Luo, and N. L. Wang, *Phys. Rev. Lett.* **101**, 257005 (2008).
- [35] D. Wu, N. Barišić, N. Drichko, S. Kaiser, A. Faridian, M. Dressel, S. Jiang, Z. Ren, L. J. Li, G. H. Cao, Z. A. Xu, H. S. Jeevan, and P. Gegenwart, *Phys. Rev. B* **79**, 155103 (2009).
- [36] L. Boeri, O. V. Dolgov, and A. A. Golubov, *Phys. Rev. Lett.* **101**, 026403 (2008).
- [37] T. Yildirim, *Phys. Rev. Lett.* **102**, 037003 (2009); *Physica C* **469**, 425 (2009).
- [38] L. Boeri, private communication.

- [39] Note that the factor of 15 reflects the number of phonon branches in BaFe_2As_2 .
- [40] T. Fukuda, A. Q. R. Baron, Sh.-I. Shamoto, M. Ishikado, H. Nakamura, M. Machida, H. Uchiyama, S. Tsutsui, A. Iyo, H. Kito, J. Mizuki, M. Arai, H. Eisaki, and H. Hosono, *J. Phys. Soc. Jpn.* **77**, 103715 (2008).
- [41] D. Reznik, K. Lokshin, D. C. Mitchell, D. Parshall, W. Dmowski, D. Lamago, R. Heid, K.-P. Bohnen, A. S. Sefat, M. A. McGuire, B. C. Sales, D. G. Mandrus, A. Asubedi, D. J. Singh, A. Alatas, M. H. Upton, A. H. Said, Yu. Shvyd'ko, and T. Egami, arXiv: 0810.4941 (2008).
- [42] R. Mittal, Y. Su, S. Rols, T. Chatterji, S. L. Chaplot, H. Schober, M. Rotter, D. Johrendt, and Th. Brueckel, *Phys. Rev. B* **78**, 104514 (2008).
- [43] M. Zbiri, H. Schober, M. R. Johnson, S. Rols, R. Mittal, Y. Su, M. Rotter, and D. Johrendt, *Phys. Rev. B* **79**, 064511 (2009).
- [44] L. Boeri, O. V. Dolgov, A. A. Golubov, *Physica C* **469**, 628 (2009).